Dyeing to Know: Harmonizing Nile Red Staining Protocols for Microplastic Identification

Derek Ho (dkho@upenn.edu)[1] & Julie Masura (jmasura@uw.edu)[2]

1 – Department of Mechanical Engineering and Applied Mechanics, University of Pennsylvania, Philadelphia, Pennsylvania 19103, United States;
Department of Biological Systems Engineering, University of Wisconsin-Madison, Madison, Wisconsin 53706, United States;
2 – Sciences & Mathematics Division, School of Interdisciplinary Arts & Sciences, University of Washington Tacoma, Tacoma, Washington 98402, United States

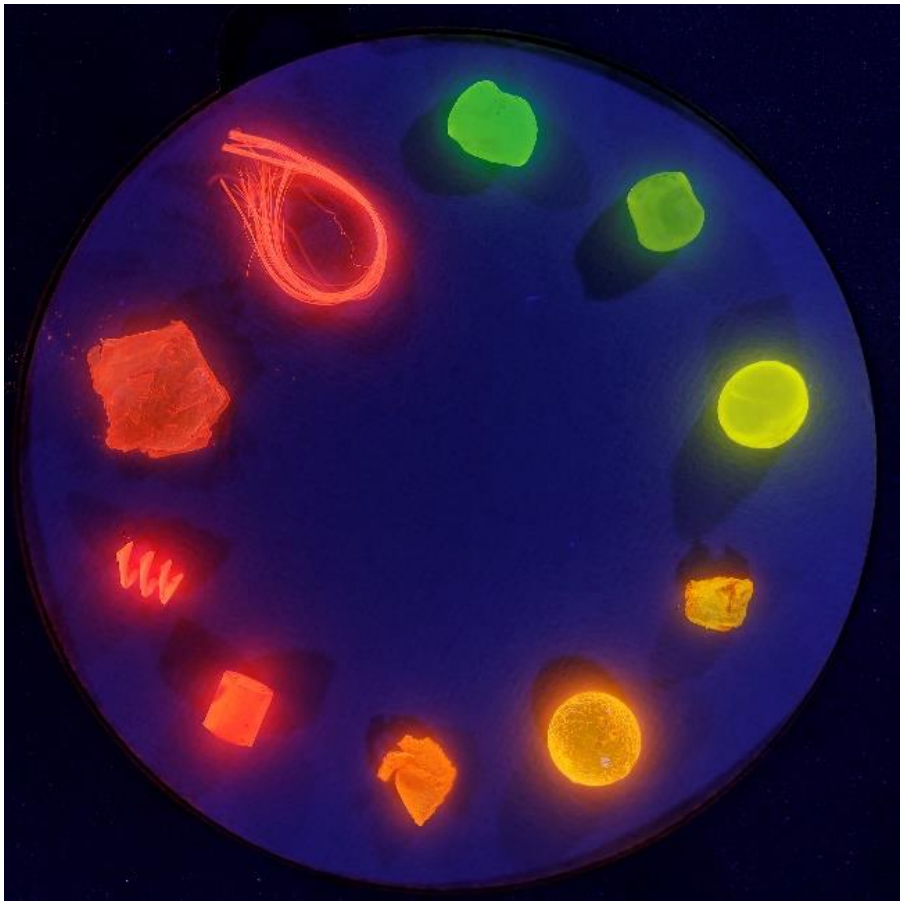

Dyeing to Know: Harmonizing Nile Red Staining Protocols for Microplastic Identification

Abstract:

With the escalation of microplastic (MPs) pollution and the laborious nature of existing MPs identification methods, new approaches for large-scale sampling of MPs in the environment are necessary. A promising solution lies in the fluorescence staining of Nile Red (NR), whose fluorescence is polarity-dependent, offering the potential for classification based on fluorescence. However, the choice of carrier solvents to dissolve NR remains unstandardized, and methods to represent and differentiate the fluorescent behavior of MPs are lacking. This study addresses these gaps by testing eight NR-carrier solvents (n-hexane, chloroform, acetone, methanol, ethanol, acetone/hexane, acetone/ethanol, and acetone/water) applied to ten most common polymer-types of MPs (HDPE, LDPE, PP, EPS, PS, PC, ABS, PVC, PET, and PA). The fluorescence behavior, including fluorescence intensity and *Stokes shift*, was compared across solvents, and their effects on polymer degradation were evaluated. Additionally, the effectiveness of various polarity measures with the proposed HSV color spaces in reflecting *Stokes shift* for MPs identification was assessed. To differentiate natural organic materials (e.g., eggshells, fingernails, wood, and cotton) from polymers, Fenton oxidation was found to quench the fluorescence of natural organic matter with minimal changes observed in NR-stained MPs. The findings identified acetone/water [25% (v/v)] as the best compromise, effectively mitigating the adverse effects of acetone while maintaining strong fluorescence behavior suitable for identification.

Keywords: Fluorescence imaging, Nile Red, Microplastics, Metrology, Polymer Identification, Polarity, *Stokes shift*

1. Introduction

The usage of plastic products has skyrocketed, climbing from 2 million tons in the 1950s to a staggering 450 million tons over 70 years [1]. This surge, notably accelerated by the Covid-19 pandemic, resulted in an estimated 8.4 ±1.4 million tons of pandemic-associated plastic waste generated globally in 2021 [2]. This influx equates to approximately 2,000 garbage trucks' worth of plastics dumped into the world's oceans daily [3]. Unfortunately, the chemical resilience that makes plastics so popular inadvertently means they do not biodegrade. Instead, they fragment through processes like UV oxidation, mechanical breakdown, and biological degradation [4], [5], [6], [7]. This fragmentation leads to smaller pieces known as microplastics (<5 mm), and eventually, nanoplastics (<1 µm).

The tiny size and omnipresence of these microplastics (MPs) enable their global transport through air and water, leading to startling discoveries in remote locations such as the Arctic ice [8], uninhabited caves [9], the highest peak of Mount Everest [10], and even the deepest parts of the Mariana Trench [11]. This increased prevalence of MPs holds profound implications for both the flora [12], [13] and fauna [14] residing in these environments. Moreover, their small size leads animals to mistake them for food, causing adverse effects such as oxidative stress, neuro- and reproductive-toxicity, and carcinogenicity [15]. Recent discoveries of microplastics in our food sources—like fruits and vegetables [16], seafood [17] and salt [18], and even water bottles [22] and food packaging [23], and their accumulation in placenta [21] and blood [22] of healthy humans —have raised concerns. With limited understanding of their profound effects on human health and projections indicating a potential doubling of microplastics in oceans within the next 30 years from 2020 levels [23], there is an urgent need for standardized monitoring approaches capable of handling large sample numbers and volumes within short periods to study spatial and

temporal distribution of MPs [24]. Such approaches are critical for comprehensive assessments, comparison and integration of research on microplastic presence across diverse environments.

The most commonly used methods for detecting and identifying MPs rely on visual assessment with the naked eye, cameras, or microscopes, followed by spectroscopic validation using techniques such as Fourier-transform infrared (FTIR) or Raman spectroscopy [25], [26]. While widely adopted, these approaches face significant limitations: they are labor-intensive, time-consuming, and prone to a high rate of false positives due to subjective operator selection criteria during MPs analysis [27], [28]. For instance, relying on distinct visual features such as color and surface structure (i.e. sharp geometrical shapes, shiny surfaces and fibers with consistent widths), often leads to the underestimation of less visually obvious plastics, such as clear, black, white, brown fragments [29]. This subjective, label-free selection process frequently results in misidentification rates ranging from 20–70% [30]. Alternative methods, such as thermal analysis techniques (e.g., thermogravimetric analysis (TGA), thermal extraction desorption (TED), pyrolysis-gas chromatography/mass spectrometry (PY-GC/MS)), have been proposed for MPs identification [31]. However, these approaches have significant drawbacks. They cannot determine the number, type, or morphology of MPs, and are unsuitable for analyzing large samples due to overlapping polymer signal peaks and lengthy analysis times (e.g., approximately 70 minutes per sample with PY-GC/MS) [25], [31], [32]. Therefore, it is critical to develop faster, more accurate, and objective methods for MPs detection and identification that are accessible to laboratories worldwide. Such advancements will improve the reliability and scalability of MPs research and monitoring efforts.

To address these challenges, researchers have turned to fluorescent labelling methods, including but not limited to, DANS, methylene blue, Evans blue and DAPI, and Nile red (NR)

[29]. Among these options, NR was selected due to its widespread adoption across international laboratories, as well as its exceptional selectivity and minimal interference in the infrared spectral region, which enables subsequent spectroscopic identification via FTIR [29]. NR fluoresces selectively, preferentially binding onto hydrophobic materials, like lipids and plastics, in polar environments, rather than inorganic materials, like sand [29]. Importantly, its fluorescence behavior varies on the physiochemical properties of the plastics, suggesting the potential to differentiate MPs based on their polarity-dependent fluorescence behaviors [33], [34], [35].

However, applying NR requires a carrier solvent to effectively disperse the dye onto MPs. Various solvents, including N-hexane, chloroform, methanol, ethanol, DMSO, Tween 20, acetone/ethanol, and acetonitrile/methanol, have been explored to optimize NR fluorescence while minimizing adverse effects, such as plastic dissolution or swelling [29]. Despite these efforts, the absence of a standardized solvent has hindered progress in the field of MPs research, leading to inconsistent results, such as the underestimation of low-fluorescing MPs, overestimation of the MPs particle count due to false positives of natural organic matter (NOM), and inaccurate particle size determination due to swelling, and lack of cross-study comparability [36].

To address these inconsistencies, researchers have attempted to investigate the underlying mechanism regarding NR partitioning onto MPs within a multiphasic system. Shim et al. (2016) proposed that non-polar solutions like n-hexane, facilitate improved partitioning of NR fluorophores onto MPs, thereby enhancing the fluorescence of MPs [37]. Conversely, Tamminga et al. (2017) found that more polar solvents, such as chloroform, produced higher fluorescence in NR-stained PE and PP compared to n-hexane [38]. This apparent contradiction highlights the

complexity of the underlying mechanism governing NR partitioning onto MPs and fluorescence behavior in a multiphasic system. As a result, developing a standardized solvent for NR staining remains a challenge, compounded by the diverse fluorescence and degradation tendencies of plastic types in different solvents.

In addition to solvent challenges, methods used to quantify and differentiate the fluorescent behavior of MPs are inadequate. Imaging devices, such as cameras, cannot capture fluorescence at discrete wavelengths (nm); instead, they interpret the perceived fluorescence as a permutation of red, green, and blue (R/G/B) channels. This limitation complicates the direct identification of MPs based on their fluorescence behavior. As a workaround, researchers commonly convert fluorescent images to monochrome and apply greyscale thresholding based on pixel brightness to isolate particles with fluorescent intensity (FI - %) above a certain threshold. While this approach enables an approximate differentiation of MPs by their crystallinity – since FI decreases with polymer crystallinity [34], [39], [40] – it is prone to false positives. For instance, NOM, such as wood and chitin [40], often exhibit a higher FI than highly crystalline plastics - polyvinylchloride (PVC) and polyethylene terephthalate (PET) [40].

To improve MPs differentiation, researchers have explored RGB-based interpretation of fluorescence, developing formulaic representations of RGB, (Red+Green/Red), (Red-Blue/Red+Blue), or even their layered combinations to create proxy ‘polarity index’ fingerprints [34], [35], [38]. However, these RGB-based approaches have shown limited success in reliably correlating solvent polarity with the *Stokes shift* in fluorescence, reducing their effectiveness in classifying MPs based on their fluorescence behavior. Without a more robust digital representation of polarity-induced *Stokes shift* of fluorescence, fluorescence imaging analyses

remain susceptible to false positives, and cannot accurately classify MPs by their fluorescent behavior.

This study seeks to address these challenges by evaluating the efficacy of the most common carrier solvents used for NR staining in accurately identifying 10 types of MPs (high-density polyethylene (HDPE), low-density polyethylene (LDPE), polypropylene (PP), polystyrene (PS), expanded polystyrene (EPS), acrylonitrile butadiene styrene (ABS), polycarbonate (PC), PVC, PET, polyamide (PA)) based on their fluorescence behavior (FI and *Stokes shift)*. Additionally, a rapid, simple, and cost-effective staining protocol applicable to environmental samples was developed, integrating Fenton oxidation and NR staining. This protocol, combined with the application of a more appropriate Hue/Saturation/Value (HSV) color space for fluorescence representation, was assessed for its ability to differentiate MPs based on polarity-induced fluorescence.

2. Materials and Methods

2.1 Sample collection for staining experiments

Ten non-colored polymer-types (HDPE, LDPE, PP, PS, EPS, ABS, PC, PVC, PET, PA) were investigated. Non-colored HDPE, LDPE, PP and ABS virgin pellets were obtained from LNS technologies, PS was obtained from Sigma Aldrich (#331651), PA was obtained from GUM Waxed floss. The other plastics (EPS, PC, PVC, PET) were obtained from post-consumer products in the form of packing peanuts, acrylic glass sheets, PVC pipes and Dawn Ultra dish soap bottles. All-purpose cotton thread was obtained from Coats & Clark, chitin was sourced from eggshells and fingernails, wood shavings from Jack pine softwood. Due to the irregular

shapes of the prepared MPs from post-consumer goods, the dimensions of the particles ranged from as thin as 0.96 mm to as long as 2.09 cm, such as in the case of PA thread. However, the average between the minimum width and maximum length of the MPs studied ranged from between ABS (3.14 mm) to PET (5.42 mm) except for PA (10.93 mm), due to the high length-breath ratio of its thread.

2.2 Staining dye solution

The five most used solvents by researchers, namely n-hexane (Hex), chloroform (Chl), acetone (Ac), ethanol (Eth), and methanol (Met) were investigated. Additionally, three equal-part solvent mixtures of acetone with n-hexane (Ac-Hex), with ethanol (Ac-Eth), and with water (Ac-W) were used to prepare NR stock solutions of 10 µg/ml. These NR-carrier solvents (Hex, Chl, Ac, Met, Eth, Ac/Hex, Ac/Eth & Ac/W) were applied to nine different types of MPs (HDPE, LDPE, PP, PS, PC, ABS, PVC, PET & PA) to assess their ability to stain MPs with NR for fluorescence imaging. The inclusion of pure water was disregarded since NR was demonstrated to be insoluble in water. Nile Red (7385-67-3) was obtained from Santa Cruz Biotechnology. N-hexane (110-54-3), chloroform (67-66-3), acetone (67-64-1), ethanol (64-17-5), and methanol (67-56-1) were obtained from Fischer Scientific company LLC. Ultrapure (Type 1) water was obtained from Synergy UV water purification system (18.2 MΩ.cm @25°C).

2.3 Fenton oxidation pretreatment

Of the several pretreatment methods available, including acid, alkali, oxidase, and enzymatic treatments, Fenton oxidation was chosen. Acid and alkali pretreatments have been shown to cause degradation and yellowing of the polymer [41], respectively. Additionally,

enzymatic pretreatment requires a lengthy digestion period [41]. As such, we adapted the Fenton oxidation pretreatment from Masura et al. (2015) [42], excluding the density separation with a salt solution to ensure the inclusion of MPs of all densities. Ferrous sulfate heptahydrate ($FeSO_4 \cdot 7H_2O$) (7782-63-0), concentrated sulfuric acid (H_2SO_4) (7664-93-9), Whatman 47mm 2.5 µm Grade 42 filter paper was obtained from Fischer Scientific company LLC. Hydrogen peroxide (H_2O_2) 30% (v/v) (7732-18-5) was obtained from Santa Cruz Biotechnology. The Fe(II) stock solution was prepared by adding 7.5g of $FeSO_4 \cdot 7H_2O$ to 500 mL of water and 3 mL of concentrated sulfuric acid [42]. To prepare the samples for Fenton oxidation, 2 ml Fe(II) stock was added to 2 ml H_2O_2 to a test tube with 3 pieces of MPs, and immersed in a water bath set at 70°C for 30 minutes in a fume hood, with periodic agitation every 10 minutes to ensure mixing. MPs were then filtered out of the Fenton solution onto the 47 mm filter paper with a membrane vacuum filtration apparatus.

2.4 NR staining of MPs

15 ml of NR solution was added to the test tube and placed into a water bath (70°C) for 30 minutes in a fume hood, with periodic agitation every 10 minutes to ensure even staining. Plastics stained with Chl were treated at room temperature in a fume hood and covered with aluminum foil for 24 hours. Subsequently, one of each of the plastic particles was selected and positioned on the 47 mm filter paper and arranged in the order of their supposed polarity. To evaluate the accuracy of the segmentation of non-overlapping particles the particles were arranged with tweezers on a 47 mm filter paper for fluorescence imaging.

2.5 Fluorescence illumination and imaging instrumentation

The NR-stained particles illuminated with a circular illumination lighting setup consisting of four 310 nm LED (CUD1GF1A) positioned equidistant 10 cm apart, placed 2 cm above the samples and emitted 0.3 lx of light (as measured by Professional LED Dr.meter Light Meter B07LF4BT8V). Images were photographed with Canon RP mirrorless camera equipped with a 100 mm f/2.8 macro lens (f/2.8, t= 15 s, ISO 100, 4072 x 4072 pixels, Colour correction= 2500 K) with a High Dynamic range (HDR) obtained using the in-built HDR function (EV±1). This resulted in a replicable captured image of absolute exposure value of EV 1±1 and fixed luminous exposure value of 4.5 lx.s.

2.6 Quantifying fluorescence behavior differences

Given the limitations of using RGB color space for polarity-dependent classification, particularly its inability to accurately represent *Stokes shift*, alternative color spaces like CIE L*u*v* and HSV were evaluated. The CIE L*u*v* color space represents color in perceptually uniform dimensions: Lightness (L*) on a scale of 0–100, chromaticity along the red-green axis (u*) and the chromaticity along the blue-yellow axis (v*), This perceptual uniformity aligns closely with human color perception, making it ideal in detecting subtle color differences. In contrast, HSV represents colors in a cylindrical model based on Hue (0–360°, corresponding to the dominant wavelength), Saturation (0–100%, indicating color purity), and Value (0–100%, denoting brightness). HSV was chosen as the color space classifying fluorescent images for several reasons: (1) Hue intuitively corresponds to the dominant fluorescent wavelength, enabling clear differentiation of fluorescence color; (2) the independence of hue from brightness ensures consistent color identification regardless of variations in illumination, aligning with the

monochromatic nature of fluorescent images; (3) Saturation effectively captures the purity of fluorescent colors, while intensity is better represented by the Value channel [43]. Together, these relationships provide a more intuitive and accurate characterization of fluorescent images, allowing for weighted emphasis on the channels, which enhances classification precision and supports improved polarity differentiation.

For each of the MPs analyzed, the HSV color was sampled using the 'eyedropper' tool in photoshop of five points within the particle (top, center, bottom, leftmost and rightmost) and averaged. To represent FI, the Value component of the greyscale image in the HSV color space, where 0 represents pure black and 100% represents pure white, was used. The greyscale and color values were obtained by averaging the HSV color data of the three stained MPs; and can be found in Table S1.

2.7 FTIR analysis of Pretreated and NR-stained MPs

Duplicates of the FTIR spectrum of the 10 MPs (Control, Fenton treated, Fenton-treated and NR-stained) were obtained using Nicolet iS50R FTIR with the IRIS ATR adapter. The spectral range of 4000–400 cm^{-1} with 50 scans, resolution of 4 and 100% aperture was used for spectral analysis.

2.8 Spectral behavior analysis of NR-stained MPs

In the absence of a spectrophotometer, a retrofitted multispectral camera with four selective bandpass filters was employed to isolate and compare fluorescence behaviors across the spectral range. Cokin optical transmission filters were used: green, yellow, orange, and red. The longpass filters had cutoff points of 510 nm (yellow), 580 nm (orange), and 620 nm (red), while

the green filter, a dual-bandpass filter, exhibited transmission peaks at 500 nm (green light) and beyond 715 nm. FI measurements of the MPs were taken at three distinct locations—center, top, and bottom—to account for intra-particle variations.

2.9 Quality Assurance / Quality Control

Attention to Quality Assurance / Quality Control (QA/QC) in microplastics research is imperative to verify accuracy of data collection, ability to compare results, and replication of investigations. Polymers purchased for this project, in general, included standard non-colored pellets from semi-transparent to opaque with sizes ranging from ~1-6 mm long dimensions. Environmental samples included non-colored eggshells, fingernails, PET bottles, and fibers cut to similar dimensions to the polymer pellets. All types were verified using FTIR analysis. Investigations were completed in a clean laboratory fume hood due to the use of volatile chemicals. The researcher wore a black lab coat in contrast to the clear to white materials used to easily identify potential contamination. When polymers were tested at least three locations were used on the surfaces of each piece. Experiments were repeated in triplicate to ensure replication of results. Due to the size of the materials used for this project, any appearance of fibers or potential polymer contaminants were manually removed to confirm clear representation of observations.

3. Results

3.1 Effects of Solvent on fluorescence behaviour

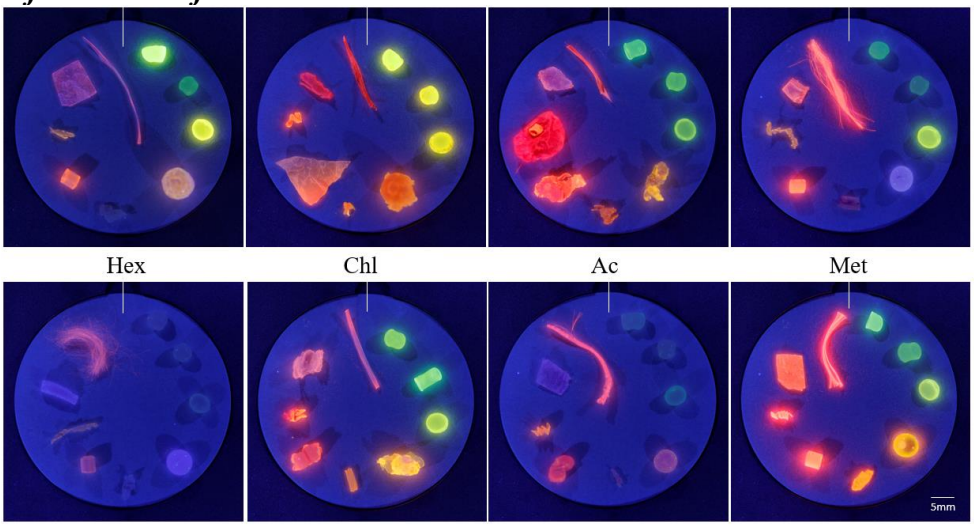

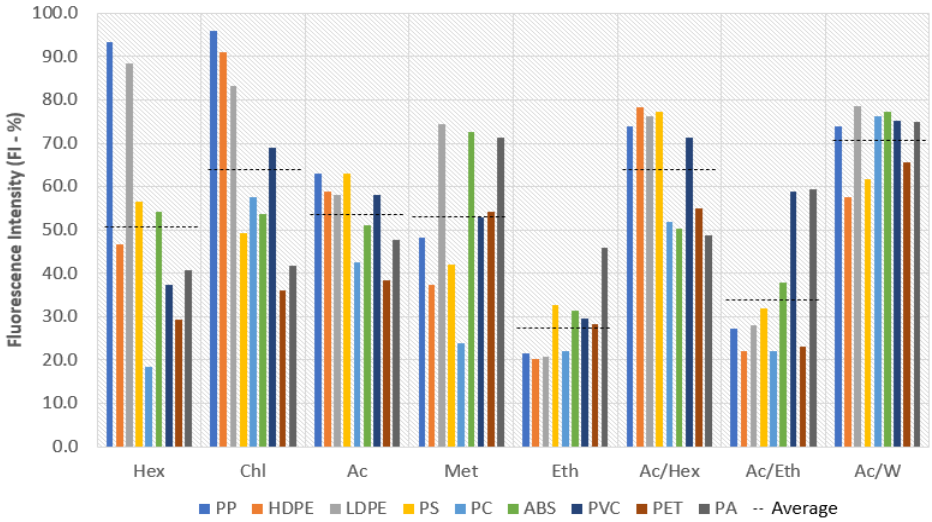

	Hex	Chl	Ac	Met	Eth	Ac/Hex	Ac/Eth	Ac/W
PP	x							
HDPE								
LDPE								
PS	x	x	x			x		
PC	x		x					
ABS	x	x	x			x	x	
PVC		x	x			x		
PET					x			
PA					x			

Figure 1a (top): NR-stained MPs in different carrier solvents - Hex, Chl, Ac, Met, Eth, Ac/Hex, Ac/Eth, Ac/W. (MPs arranged clockwise, starting from the top right of the white line: PP, HDPE, LDPE, PS, PC, ABS, PVC, PET, PA).
Figure 1b (middle): Fluorescence intensity (%) of NR-stained MPs of Figure 1a of different solvents. Dotted line indicates the average FI (%) across all MPs of the carrier solvent.
Figure 1c: HSV color representation of NR-stained MPs of Figure 1a arranged by polarity. A cross symbol (x) was used to signify any degradation by the solvent. (HSV values found in Table S1)

To assess the effectiveness of NR-carrier solvents (Hex, Chl, Ac, Met, Eth, Ac/Hex, Ac/Eth & Ac/W) on eliciting fluorescence in MPs, one stained MPs of each solvent were arranged clockwise (see Figure 1a), starting with PP (top, right of line), followed by HDPE, LDPE, PS, PC, ABS, PVC, PET & PA (top, left of line). The optimal NR carrier solvent will be evaluated as one that is able to (i) elicit strong FI across all the MPs studied, (ii) minimal polymer degradation and (iii) reflect the polarity-induced *Stokes shift* of MPs.

Among the pure solvents studied, Chl exhibited the highest average FI for the nine plastics (FI: 64.2%), followed by Ac (53.4%), Met (53.0%), Hex (51.7%), and Eth (28.1%), as shown by the dashed lines in Figure 1b. This order deviates from the expected trend based on solvent polarity, where highly non-polar solvents was expected to enhance NR partitioning onto the MPs, thus supposedly increasing fluorescence (e.g., Hex > Chl > Ac > Met > Eth).

Within individual solvents, the FI of the MPs varies depending on their molecular interactions with the solvent. In Hex, aliphatic MPs (e.g., PP (93.3%) & LDPE (83.3%), except for HDPE (46.7%) due to its high crystallinity), exhibit stronger FI than the other MPs, especially PC (18.3%). However, some MPs in Hex, like PP and PS, experience adverse swelling due to the expansion of the polymer matrix and making these plastics appear larger. In Chl, most MPs exhibit strong fluorescence, with PET showing the lowest FI of 36.0%. Despite the promotion of FI of all MPs, Chl induces adverse degradation in many MPs, particularly causing complete dissolution of those with aromatic groups (PS, ABS, and PC), swelling certain MPs like PET and PVC. MPs stained with Ac also exhibit strong fluorescence across all MPs, with PET showing the weakest FI of 38.3%. However, Ac induces dissolution of MPs with aromatic groups (PS, ABS, PVC) and swelling with PC and PET. In Met, most MPs elicit fluorescence greater than 37.3%, except for PC (24%), whereas in Eth, the MPs (PP, HDPE, LDPE, PC)

barely elicit fluorescence, with some plastics PS, ABS, PET, only visible due to their autofluorescence.

The disparity in FI (Met: 53.0% & Eth: 28.1%) is notable considering that these alcohols, Met and Eth, share a similar hydroxyl functional group, which is known to quench fluorescence [44], yet exhibit significantly different FI. This variance in FI could be attributed to the smaller molecular size of Met (3.80 Å) [45] compared to Eth (4.14 Å) [46], facilitating better absorption of NR into the polymer matrix. Unlike Met, which did not result in any observable degradation, Eth-stained PET and PA appeared to swell and unravel respectively. It is worth noting that the background filter's FI is 20%, making some MPs, such as PC (18.3%) in Hex, PC (24%) in Met, and PP (21.7%), HDPE (20.3%), LDPE (20.7%), PC (22%) in Eth, difficult to distinguish from the filter paper using standard greyscale thresholding techniques.

In addition to concerns FI and polymer degradation, it is crucial to consider how accurately fluorescence reflects the polarity-induced *Stokes shift* of the plastic. Figure 1c provides insight into this *Stokes shift*, presenting the average color samples of the plastics (Figure 1a) arranged in ascending polarity. Utilizing the HSV (Hue/Saturation/Value) color space, where primary colors - red (0°), green (120°), and blue (240°) - can help us better understand the effects of polarity-induced *Stokes shift*. It is expected that MPs with higher polarity would exhibit a more significant red-shift (counter-clockwise degree shift). Analyzing the solvents with a strong, consistent FI, it was found that Ac and Chl are the only two solvents reflecting the anticipated evolution of red-shift in polarity from PP to PA (refer to Figure 1c and Table S1). The colors of PP to PA evolve from green (154°) to red (339°) in Ac and yellow (73°) to red (351°) in Chl, resulting in a spectrum range difference of 82° and 175°, respectively. This difference in spectrum range is attributed to the solvent-dependent polarity-shift of Chl, making all MPs,

especially aliphatic ones (PP, HDPE, LDPE), appear more red-shifted. For instance, compared to PP in other solvents (Hex's 91°, Ac's 154°, and Met's 180°), which appears green, PP in Chl experiences a red-shift, appearing yellow (73°).

In summary, each pure solvent studied possesses unique advantages and disadvantages as an NR carrier solvent for a wide range of MPs. Hex, despite being the most non-polar solvent, falls short in yielding the strongest FI and induces adverse swelling in some plastics. Chl exhibits the strongest FI for all MPs but causes complete deformation in plastics with styrene groups (PS and ABS) and PVC. Alcohols (Met and Eth) show limited degradation but poor fluorescence across most polymers. Although not as bright as Chl and with some dissolution of the polymer structure, Ac has been proven to induce fluorescence in all nine MPs studied. Furthermore, the extended color spectrum of Ac makes it more suitable for clearly distinguishing between plastics. To enhance the applicability of solvents to a broader range of polymers while mitigating adverse effects, the mixing of Ac with other solvents was explored to enhance NR staining and the fluorescence of MPs.

3.2 Solvent Mixtures

Ac was mixed with three solvents possessing distinct chemical properties, specifically, (i) non-polar solvent n-hexane, (ii) highly polar solvent water, and (iii) moderately polar ethanol [47]. It is believed that the combined properties of these solvent pairs could elicit greater NR partitioning or lower degradation. The TEAs graph was used to illustrate the three component forces of solubility interactions: hydrogen bonding force (fh), polar forces (fp), and dispersion force (fd), projected on a triangle plot to represent their relative component contribution to the total Hildebrand value [48]. The TEAs graph is often used to predict and formulate solvent

mixtures with different chemical properties through interpolation between the solvents qualitatively assess the effect of solvents on polymers [48].

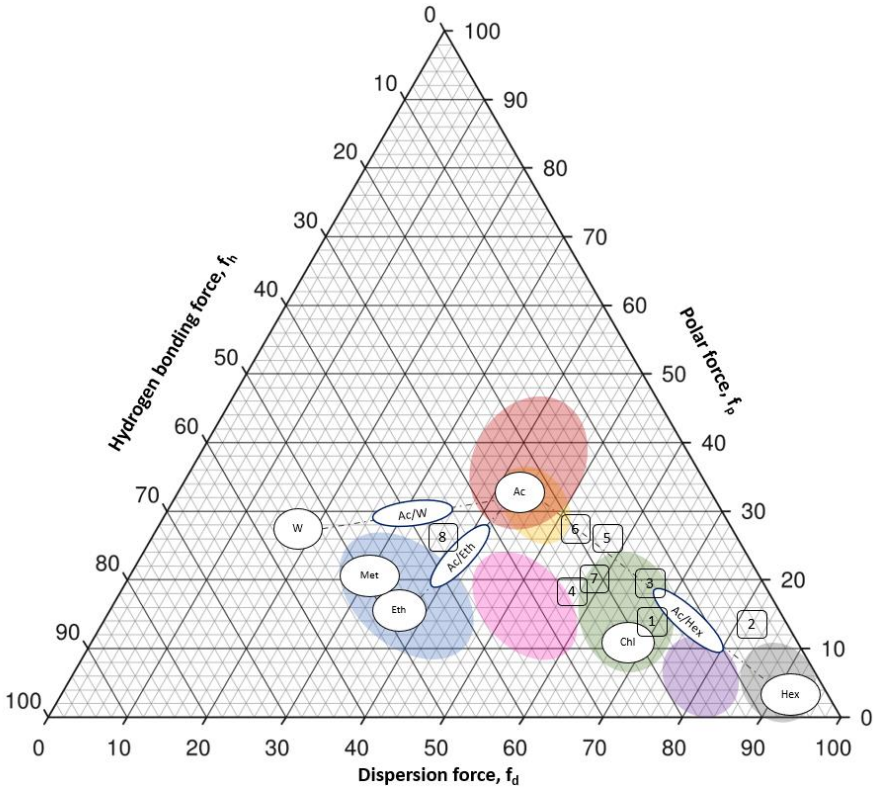

Figure 2: TEAs graph illustrating solvent class and its polymer solubility windows. Solubility windows are indicated in color shaded circles (Blue-alcohols, yellow – ketones, red- amines, gray- aliphatic, green – chlorine, purple – aromatics, pink – esters), solvents are represented by the lettered circles (Ac, Chl, Hex, Met, Eth, W, Ac/W, Ac/Eth, Ac/Hex) and the plastics are represented in numbered squares (1-PE, 2- PP, 3-PS, 4-ABS, 5-PC, 6-PVC, 7-PET & 8 – PA).

The adapted TEAs graph [48] (see Figure 2) illustrates the relative positions of solvents and polymers, enabling their classification into solvent classes within arbitrarily shaded regions—alcohols (blue), ketones (yellow), amines (red), aliphatic (grey), chlorine (green), aromatics (purple), and esters (pink). These shaded regions, referred to as "polymer solubility windows," were empirically derived by researchers who charted the proximity of a polymer to particular region(s) indicating potential solubility in those solvents [48]. By adapting the regions of solubility windows [48] and superimposing the positions of solvents (circles) and polymers of interest (squares) [49] onto the TEAs graph (refer to Table S2), the effect of solvents on

polymers can be qualitatively assessed. For example, in Figure 2, it can be observed that the proximity of ABS, PS, PVC, PET, and PE in the green shaded region where Chl resides, indicates a high degree of chemical compatibility in Chl, resulting in greater swelling/dissolution. This dissolution rate aligns with our observed deformation (as evident in Figure 1a) of ABS, PS, PVC, PET. It is noteworthy that due to the focus on the interaction of solvents with the amorphous regions of polymers, the TEAs graph may not fully represent the effect of higher ordered crystalline structures (i.e., HDPE vs LDPE) and the absence of reactive groups (PE and PP) that make some plastics chemically resistant to solvents. Despite the potential of the TEAs graph to help visualize the solubility of polymers in solvents, caution must be exercised as it is a 2-dimensional simplification of complex chemical compatibility and it excludes important factors like temperature (>25°C), concentration of solvents (>10%), and exposure time [48].

Compared to just Hex, the addition of Ac to Hex improved the FI of several MPs (Average FI: 64.8%), namely PC (52.0%), PVC (71.3%), and HDPE (78.3%). However, this Ac/Hex mixture also resulted in enhanced dissolution of the polymer matrix of PS, ABS, PVC, and PET, as well as swelling of HDPE (See Figure 1a). These more pronounced adverse effects can be explained by the TEAs graph (Figure 2), which positions the Ac/Hex mixture in a region proximate to where most of the investigated polymers lie, resulting in higher compatibility for solubilization.

The mixture of Ac/Eth improved the fluorescence of several MPs (average FI: 27.3%), specifically PS (32.0%), ABS (38.0%), PVC (59.0%), PA (59.3%), and to a limited degree PP (27.3%), LDPE (28.0%), PC (22.0%), and PET (23.0%), compared to pure Eth. Though improved, the FI of the Ac/Eth remains suppressed due to presence of the fluorescence

quenching properties of the ethanol. However, the Ac/Eth mixture did mitigate against the dissolution of all the plastics and even maintained the integrity of the wax of the PA fibers.

Lastly, the Ac/W mixture was found to elicit the strongest fluorescence across all the 9 MPs (average: 71.3%), compared to all solvents studied. In addition to this improved FI, specifically PS, PC, and PET, the Ac/W demonstrated a reduction in the degradation of PS, ABS, PC, and PVC, as reflected by their increased distance away from these MPs in the TEAs graph. Despite water being more polar and exhibiting stronger fluorescence-quenching hydrogen bonding than Eth, it was found that Ac/W elicited greater fluorescence than Ac/Eth. It is suspected that the smaller molecular size of water (1.62 Å) relative to the 4.14 Å of Eth and 4.19 Å of Ac [46] promoted greater penetration of NR into the polymer matrix, improving fluorescence. Therefore, after comparing the three different Ac/mixtures, it is concluded that Ac/W appears to be the best compromise eliciting strong fluorescence with minimal degradation and will be used in further investigation.

3.3 Optimizing Ac/W mixtures

To optimize the Ac/W mixture, a combination of Ac/W ranging from 10-70% acetone, with the rest containing water, was investigated. These Ac/W solvent mixtures were tested on the MPs most sensitive to degradation – PS, PC, ABS, PVC and PET; with expanded PS (EPS) added to ensure better applicability to MPs with different crystallinity (see Figure 3). The MPs were arranged in a clockwise fashion with 10% (top, right of line) to 70% (top, left of line). In Figure 3a, it was observed that at low concentrations of Ac/W, specifically at 10% (right of the line), there was minimal fluorescence visibility of EPS and PC. With increasing concentration of Ac in the mixture, there was a noticeable red-shift in the NR fluorescence, intensifying to its

reddest state at Ac/W 70%. Additionally, at higher concentrations, EPS appeared to shrink in size due to its tendency to dissolve in Ac. However, as the concentration of Ac increased, the greater the degree of malformation of the MPs, resulting in the fusion with neighboring MPs, such as in the case of PS (Ac >30%) and ABS (Ac >40%), and the warping of PET (Ac >60%).

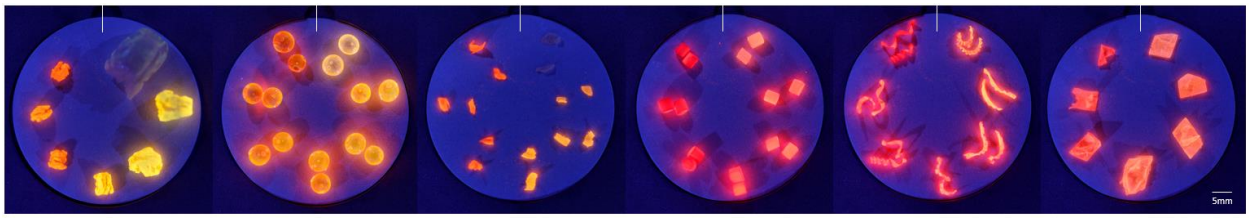

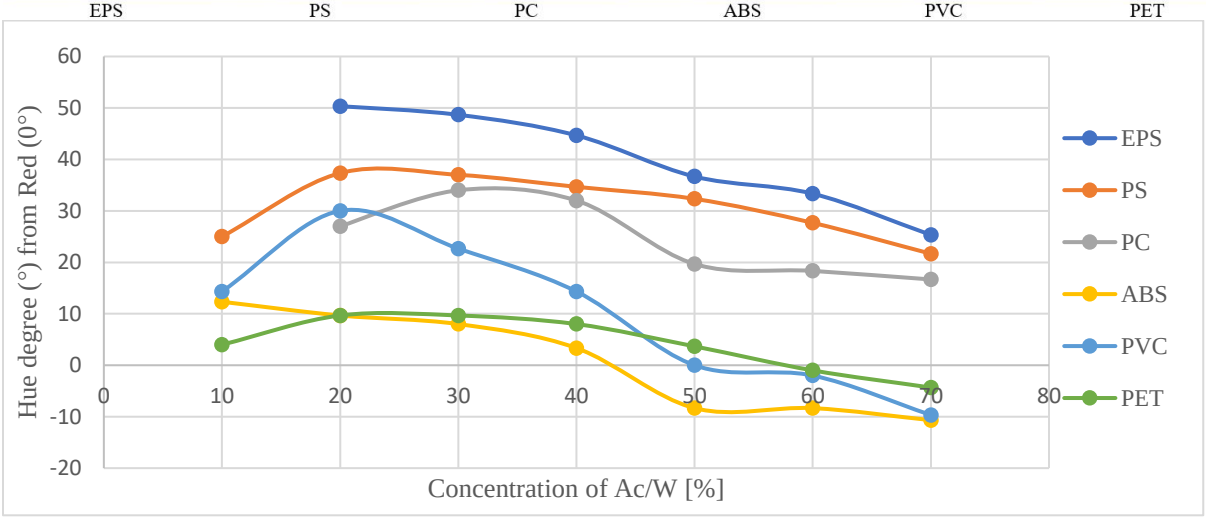

Figure 3a (top): Ac/W mixture of 10 – 70% for EPS, PS, PC, ABS, PVC and PET (Topmost (clockwise): 10, 20, 30, 40, 50, 60, 70% W:Ac mix)
Figure 3b (bottom): Comparison of the deviation of dominant hues (°) of EPS (dark blue), PS (orange), PC (gray), ABS (yellow), PVC (blue) and PET (green) across Ac/W mixture of 10 – 70%. Points below the horizontal axis reflect hue values below 360°, whereas any values above indicate values greater than 0°.

To investigate how the color of the MPs changes with Ac/W concentration, a graph (Figure 3b) displaying the deviation of dominant hues (°) of the 6 MPs from red (0/360°) against increasing concentrations of Ac/W (ranging from 10% to 70%) was plotted. Here, negative y-axis values indicate hue values smaller than 360°, while positive values indicate values above 0°. Data points of EPS (-63°) and PC (-65°) of Ac/W at 10% were excluded due to their lack of fluorescence. In Figure 3b, it was found that certain plastics exhibited distinct hue peaks, such as PS (25%), PVC (20%), PET (25%), and PC (30%), indicating dominant hues before a red-shift

(decreasing hue) occurred with increasing solvent polarity. Considering the range of dominant hue peaks and the tendency for solubilization at higher concentrations of Ac, it appears that an Ac/W mixture between 20–30% is suitable. Therefore, a compromise of 25% as the concentration of Ac/W was deemed to be the most optimal solution for reflecting polarity-induced fluorescence.

3.4 Classification using Polarity-induced fluorescence

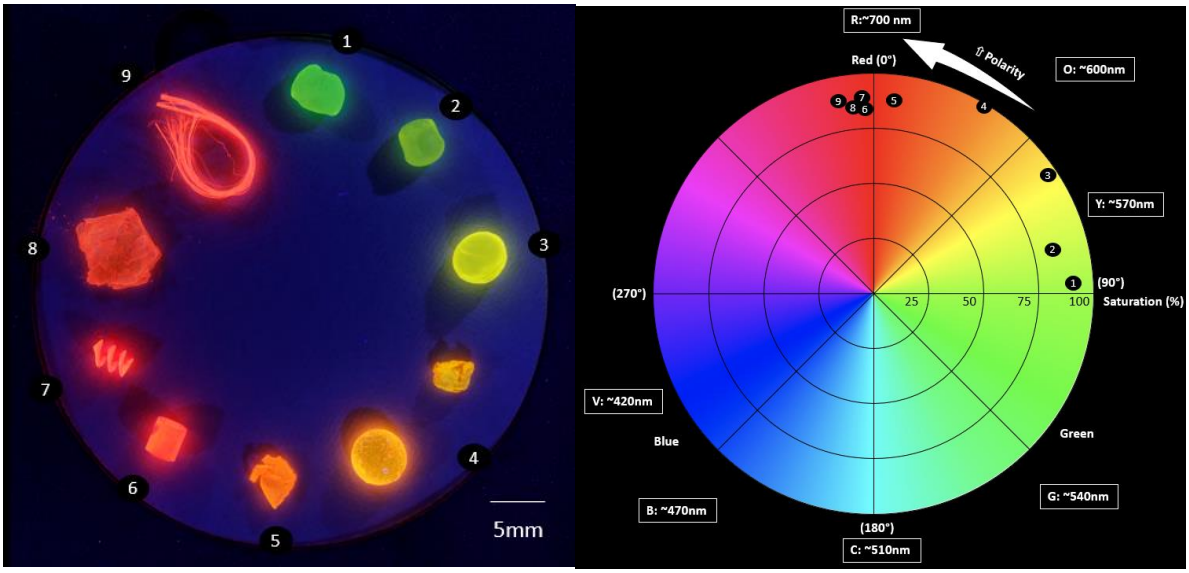

Figure 4a (left): 10 MPs stained with NR [10 µg/ml] dissolved in Ac/W mixture of 25% at 70°C for 30 mins, captured at absolute exposure value of EV 1±1 and luminous exposure value of 4.5 lx.s. (From top, clockwise – 1.PP, 2.HDPE, 3.LDPE, 4.EPS, 4.PS, 5.PC, 6.ABS, 7.PVC, 8.PET, 9.PA)

Figure 4b (right): Simplified two-dimensional HSV color wheel (Hue (360°) & Saturation (radial axis -%) without Value projections) of NR-stained MPs labeled in Figure 4a. As the polarity of MPs increases, the Hue of the MPs is red-shifted counter-clockwise. Plastics with higher saturation (%) would appear further away from the center of the color wheel. (From Rightmost, anti-clockwise – 1.PP, 2.HDPE, 3.LDPE, 4.EPS, 4.PS, 5.PC, 6.ABS, 7.PVC, 8.PET, 9.PA)

To ensure environmental applicability and accurate correlation of these measures of polarity with the fluorescence of NR-stained MPs, ten types of MPs (PP, HDPE, LDPE, EPS, PS, PC, ABS, PVC, PET & PA) were subject to Fenton-oxidation pretreatment and stained with a 25% Ac/W mixture. The MPs were then arranged in a clockwise fashion based on their hue (see Figure 4a). A simplified 2D representation of the 3D HSV color space of the MPs was

created, illustrating the angular position of Hue (360°) of the color wheel, with the outward radial axis representing saturation (%) (without the dimension of Value), as shown in Figure 4b. The plastics are labelled according to their increasing red-shift in dominant wavelength, ranging from green to red — #1.PP, #2.HDPE, #3.LDPE, #4.PS+EPS, #5.PC, #6.ABS, #7.PVC, #8.PET, #9.PA. A clear trend in the red-shift of the fluorescence of MPs is evident in the counter-clockwise progression of the dominant hue (°), from green PP (#1) to red PA (#9), as depicted in Figure 4b.

Polarity, defined as the imbalance in electronegativity among molecules and atoms, can be assessed through physical surface properties like water contact angle (WCA) and dielectric charge, or approximated using chemical properties such as partitioning coefficients, as summarized in Table 1. WCA measurements below 90° indicate hydrophilic characteristics, while values above 90° suggest hydrophobicity [50]. Dielectric constant (DE) measures the material's ability to polarize under an electric field, with higher DE indicating greater polarity [51]. Molecular-level indicators like partitioning coefficients between octanol and water (log K_{ow}) also inform about polarity, with computational models offering reliable estimates [52].

Table 1: Measure of polarity: water contact angle (WCA), dielectric constant (DE) and partitioning coefficient (log K_{ow}) with increasing degrees of polarity

WCA [50]	DE [51]	log K_{ow} [52]
PP (102.1°)	PP (2.3)	PP (23.7)
PE (96.0°)	PE (2.3)	PE (23.6)
PS (87.4°)	PS (2.55)	PS (22.9)
PVC (85.6°)	ABS (2.95)	-
PC (82.0°)	PC (3.3)	PC (21.3)
ABS (80. 9°)	PVC (3.55)	PVC (16.2)
PET (72.5°)	PET (3.5)	PET (8.1)
PA (68.3°)	PA (4.5)	PA (4.5)

3.5 Evaluating the classification ability of MPs

To assess the classification potential of NR staining, the expression, $\Delta E = \sqrt{\Delta H^2 + \Delta S^2 + \Delta V^2}$) [53] was used, to calculate the difference between two colors by assessing variations in their Hue, Saturation, and Value components among the 10 Fenton-oxidized NR-stained MPs (Table 2). This ΔE value, facilitates precise evaluation of color dissimilarity, with fluorescence yielding larger ΔE values more easily distinguishable due to greater color disparity. The minimal detectable difference in color is a ΔE of 1, with values between 3–6 indicating noticeable differences in color. A range of 6–10 suggests perceivable color differences that are noticeable to most people, while values above 10 denote substantial and significant differences [54], [55]. It's important to note that ΔE is particularly adept at discriminating between colors rather than matching them.

Table 2: Comparison of ΔE between MPs investigated.

ΔE between MPs	**PP**	**HDPE**	**LDPE**	**EPS**	**PS**	**PC**	**ABS**	**PVC**	**PET**	**PA**
PP		17.3	37.7	57.6	61.2	74.2	90.3	90.1	88.1	91.8
HDPE			29.5	46.6	51.7	63.8	80.4	80.7	74.9	82.4
LDPE				20.5	24.2	37.1	55.5	56.5	55.2	59.2
EPS					10.1	18.8	39.7	42.1	38.3	45.5
PS						13.3	32.2	34.0	35.5	37.5
PC							22.0	25.4	26.6	29.5
ABS								5.4	22.1	9.5
PVC									24.3	4.7
PET										24.7
PA										

Red (ΔE: 3-6) = Noticeable differences in color
Orange (ΔE: 6-10) = Moderate color differences that are readily noticeable by most people
No color (ΔE > 10) = Substantial differences and considered easily distinguishable

The majority of the 10 MPs can be easily distinguished from one another (ΔE >10). Notably, there is a moderate capability to differentiate between PA and PVC (ΔE: 9.5), while the ability to distinguish PVC and ABS is diminished (ΔE: 5.4), as well as PVC and PA (ΔE: 4.7). The

limitations in clearly distinguishing between PA, PVC, and ABS are believed to stem from the use of a digital camera to capture fluorescent colors.

To investigate the effects of Fenton-oxidation on the fluorescence of MPs and NOM, ten different MPs and common NOM sources - derived from chitin (eggshells and fingernails), wood shavings, and cotton- were examined. Both NR staining with and without pre-treatment were compared, and the particles were arranged in a clockwise fashion to prevent overlap (refer to Figure S1). The respective ΔE values between NR staining with no pre-treatment (control) and Fenton oxidation are summarized in Table S3.

It was observed that Fenton-oxidation resulted in minimal changes to the fluorescence of NR-stained MPs, with ΔE ranging from 2.5 (PA) to 9.8 (ABS) (refer to Table S3). In contrast, most NOM exhibited a significant reduction in fluorescence, with chitin (fingernail: ΔE = 38.0, eggshell: ΔE = 59.0) and wood (ΔE = 60.5) experiencing complete quenching of fluorescence. Cotton showed a lesser reduction (ΔE = 11.9), but still exhibited fluorescence after Fenton oxidation. Notably, cotton's purple hue (254°) remained distinct from the spectrum of NR-stained MPs (ranging from red to green, 352°–87°), allowing it to be easily differentiated from MPs. Despite some decrease in FI, all studied MPs retained their dominant fluorescent hue, with only a slight apparent decrease in FI.

The FTIR spectra of the 10 MPs subjected to different treatment were also examined, including the control group (without Fenton-oxidation or staining), NR-stained MPs (without Fenton-oxidation), and NR stained MPs subjected to Fenton-oxidation (see Figure S2). Among the 10 MPs, minor changes were observed in the FTIR spectrum of PVC, specifically a shift in the carbonyl stretching at 1700 cm^{-1}, while a new peak emerged in PET, corresponding to hydroxyl stretching at 2900 cm^{-1}, following NR staining and Fenton-oxidation. These oxidation-

related peaks suggest that Fenton-oxidation may induce a greater degree of red-shift in certain polymers. However, despite these changes, there were no significant alterations in the fluorescence behavior, particularly in the hue of all NR-stained MPs, as indicated by their color change ($\Delta E < 6$). This suggests that Fenton-oxidation preserves the fluorescence behavior of MPs ($\Delta E > 10$) while reducing the detection of fluorescence from NOM, such as chitin and wood. Thus, Fenton-oxidation shows promise as a method for minimizing false positives associated with NR-stained NOM in environmental studies, without resulting in polymer deformation.

3.6 Spectral behavior of NR-stained MPs

The perceived colors of MPs result from the combination of a broad spectrum of fluorescence wavelengths condensed into a single-color representation. This can lead to spectral overlap, making it challenging to distinguish MPs under certain lighting conditions—a phenomenon known as metamerism [56]. To address this, Cokin optical transmission filters (green, yellow, orange, and red) were used to isolate specific spectral ranges of fluorescing MPs. These filters function by blocking specific wavelengths while allowing those longer than their respective cutoff points to pass through. FI measurements across the four optical filters were obtained and compared side by side to generate a spectral graph, as shown in Figure 5. The FI observed with the green filter was lower than that of the other filters due to the blocking of wavelengths between its two transmission peaks. Additionally, variations in particle shape, thickness, and opacity contributed to larger standard deviations in FI measurements. Notably, PS, PET, and PC exhibited more intense fluorescence at their edges compared to their interiors.

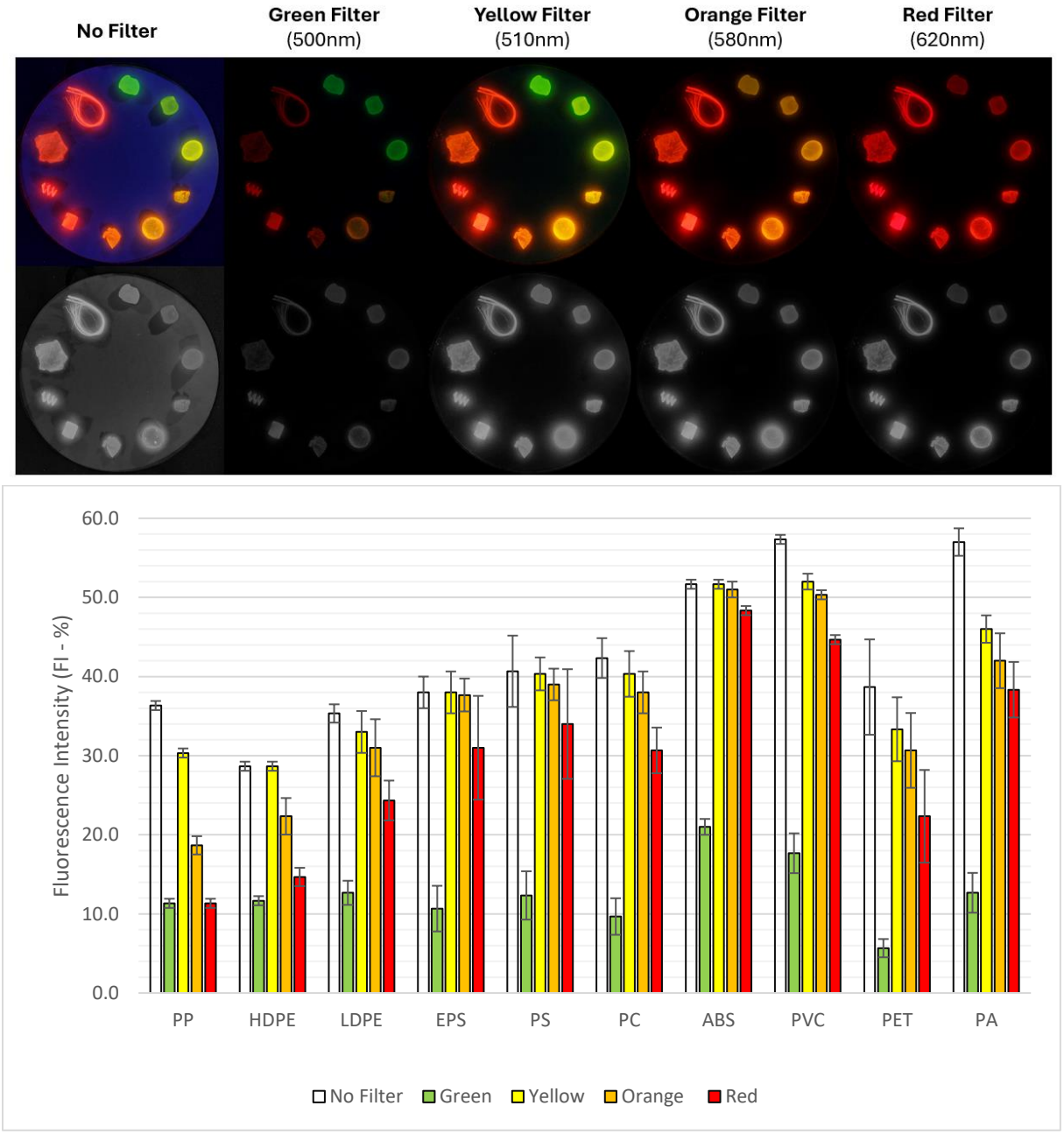

Figure 5: Fluorescence Intensity across five optical filters conditions (none, green, yellow, orange and red) of 10 MPs (PP, HDPE, LDPE, EPS, PS, PC, ABS, PVC, PET and PA) excited at 310nm.

4. Discussion

This study evaluated eight different carrier solvents to identify the most effective carrier solvent for NR-staining of MPs. Previous suggested solvents, such as Chl [38], and Hex [37], caused significant polymer degradation to certain MPs types. Solvent mixtures, such as Ac/ Eth [47], reduced degradation but resulted in limited FI. In contrast, the proposed method of using Ac/W mixture (25% (v/v) acetone) successfully mitigated polymer degradation/swelling while achieving the strongest FI (%) and the most appropriate *Stokes shift* across all the MPs. Moreover, this study demonstrated that fluorescence induced by polarity is influenced by the functional group of the MPs, rather than solely on the solvent polarity, challenging prior claims by Shim et al. (2016) [37].

In general, the three measures (WCA, DE, and log K_{ow}) act as reasonable approximations for polarity differences between polymers, distinguishing between highly polar plastics (PA/PET) and non-polar ones (PE/PP) [57]. However, discrepancies emerge in the rankings compared to the hues in Figure 4a, as observed with DE, where ABS appears more red-shifted than expected, and in WCA, where PVC appears less red-shifted than anticipated (refer to Table 1). These variations could be attributed to the limitations of these polarity measures in quantifying the specific effects of molecular groups, such as π-π bonding and hydrogen bonding, as they were originally designed to gauge their impact on specific measures of hydrophobic interactions [49, 50].

Specifically, WCA, intended as a direct measure of surface-specific hydrophobicity with water, is influenced by surface roughness, chemical composition, and any surface treatments or contaminants (additives/plasticizers). The substantial composition of 15–50% plasticizers of PVC [58] can significantly affect its surface wettability, potentially explaining the more non-

polar interpretation via WCA. On the other hand, measures like DE quantify the polarizability of the material's molecules and their response to an electric field. The presence of chloride atoms contributes to the overall polarizability of the material, thereby elevating its perceived measurement of polarity compared to WCA. However, DE, which assesses the changes in electric polarity within the molecule, exhibits less sensitivity to symmetric aromatic groups compared to polar functional groups (e.g., hydroxyl or carbonyl groups) in an electric field [59]. This reduced sensitivity stems from the delocalization of electrons in aromatic rings, thereby decreasing the magnitude of induced polarity of the molecule [60]. This limitation results in DE's diminished ability to account for π-π interactions and the perceived red-shift due to the presence of aromatic groups, potentially overlooking the molecular interaction of plastics like ABS. It is to be noted that log K_{ow} data for ABS was unavailable, but appears to exhibit similar trends as DE.

Despite the inability to account for π-π interactions, it is believed that DE and log K_{ow} can serve as a more accurate approximation for polarity than WCA. This is because WCA measures surface properties, which are sensitive to ambient humidity during measurement [61] and can be significantly reduced due to biofouling [62] and photo-oxidation [57]. In contrast, DE and log K_{ow} are designed molecular-level properties, focusing on chemical interactions with NR rather than superficial surface wettability, making them more suitable for studying NR molecular interactions. Between the two measures, the creation of a polarity catalog of MPs using log K_{ow} may be more viable than DE. This is because the contributions of the individual modes of polarization – electronic, atomic, and orientational – depend on the frequency of the electric field [59], with lower contributions from orientation and atomic polarization at higher frequencies [63]. In addition to the frequency used, the surrounding environmental conditions [64], and the geometry and thickness of the samples can affect the magnitude of DE, leading to discrepancies

between the measured induced charge of the polymers [59], [65], [66]. Hence, caution is required when selecting the database to quantify and compare DE. On the other hand, log K_{ow} values are calculated via molecular dynamic simulation from molecular models corrected to surface area, enabling comparison [52]. With an expansive database of plastics of over 110 plastics featuring different branching and chemical structures of commercial and laboratory-made polymers [52], log K_{ow} can be used to compile simulations for better understanding of molecular interactions.

Fenton-oxidation proved to be effective for eliminating the fluorescence of NOM, while causing minimal changes to the fluorescent hues and chemical properties of the MPs. This critical step significantly reduces interference of NOM (wood, chitin and cotton) in MPs detection, thereby enhancing the specificity of NR-based imaging methods. The observed quenching of NOM fluorescence is likely due to the presence of Fe(II) in the Fenton-oxidation, as metal ions are known to quench fluorescence [67]. It is hypothesized that the Fenton-oxidation partially digests NOM, leaving incompletely digested NOM with Fe(II) sorbed onto its surface. When stained with NR, the Fe(II) on NOM likely inhibits the fluorophore's ability to fluoresce, leading to fluorescence quenching. This demonstrates that the common practice of using Fenton oxidation to digest NOM not only remains compatible with Nile Red staining but also enhances its selectivity for MPs over NOM, reducing false positives, which is critical for the reliable classification of MPs in complex environmental samples.

After standardizing the carrier solvent for optimal polarity-induced fluorescence, the weighted HSV color space was introduced to improve data interpretation. Unlike the interdependent RGB color model, which requires a formulaic approach to derive a proxy "polarity index," [34], [35], [38] the hue-dominant HSV model directly correlates hue shifts (in degrees) with the perceived *Stokes shift*. This proposed HSV method allows fluorescence hue

changes to be compared intuitively, bypassing the non-intuitive relationships inherent in the RGB model. This approach is particularly valuable for environmental MPs, which often exhibit fluorescence red-shifts over time due to weathering [52], [68]. Such shifts are naturally and intuitively captured by changes in the hue channel. Moreover, in machine learning applications—where the quality of input data directly impacts the relationships deduced by the model—the weighted features and intuitive correlations of the hue channel enhance the model's ability to capture meaningful relationships. This reduces dependence on arbitrary proxies, such as those employed by Meyer et al. (2022) [69], who used decision trees to classify MPs by their individual R/G/B channels. Consequently, machine learning models leveraging the HSV-based approach can minimize noise and overfitting, significantly improving their robustness and applicability to environmental samples and large datasets.

To further enhance MPs differentiation, this study demonstrated the utility of selective bandpass filters in revealing distinct differences in fluorescence behavior, thereby improving MPs classification. This approach leverages the correlation between FI and spectra peaks [70], allowing for the determination of FI across specific wavelengths bands. As shown in Figure 5, each MPs type exhibited unique spectral profiles, indicating that differentiation based on spectral shape and intensity is feasible with the use of optical filters. This increased specificity is particularly beneficial for MPs that were previously difficult to distinguish—such as ABS, PVC, and PA—which displayed metamerism under unfiltered conditions. By applying optical filters, the emission behavior of these MPs can be isolated at specific transmission wavelengths, enabling differentiation based on their material-specific spectral characteristics.

Although higher-order statistical comparisons among multivariate datasets are beyond the scope of this study, employing statistical models to analyze fluorescence behavior (e.g., in HSV

color space) is anticipated to further enhance the accuracy and specificity of MPs differentiation. Additionally, since the fluorescence spectra of NR-stained MPs vary with excitation wavelengths [70], combining multiple excitation sources with selective bandpass filters could pave the way for developing an advanced multispectral imaging device for precise polymer identification. These findings suggest that multispectral fluorescence imaging, when integrated with machine learning, holds significant potential as a standalone method for accurate MPs identification.

As NR staining becomes a cornerstone tool for labeling MPs internationally [24], standardizing the NR carrier solvent and demonstrating its applicability for polymer identification are essential for interlaboratory harmonization. When combined with multispectral fluorescence imaging, this cost-effective method shows significant potential as a standalone approach for differentiating MPs based on physicochemical properties. However, as plastic diversity increases, further research is needed to address the effects of environmental weathering, pigments, and additives on NR fluorescence behavior. Overcoming these challenges will be critical to establishing NR fluorescence imaging as a reliable and robust method for the accurate identification of MPs in environmental samples.

5. Conclusion

In conclusion, this study systematically tested eight different carrier solvents for NR-staining of MPs and evaluated their effects on the fluorescence behavior and degradation of ten polymer types (PP, HDPE, LDPE, PS, EPS, ABS, PC, PVC, PET, PA). Through qualitative assessment of polymer degradation and analysis of hue evolution across different concentrations of Ac/W [10–70%], Ac/W [25%] was identified as the optimal solvent for enhancing fluorescence while preserving polymer integrity. Additionally, the impact of Fenton-oxidation on

the NR-staining method was investigated for both MPs and NOM. The results revealed significant fluorescence quenching in NOMs (eggshells, fingernails, wood, and cotton) with minimal changes observed in the NR-stained MPs, showcasing the method's suitability for environmental sampling applications.

This study also introduced the use of the HSV color spaces for a more appropriate representation of NR fluorescence and compared different polarity measures (WCA, DE, and Log K_{ow}) with the perceived *Stokes shift* of NR-stained plastics. The findings indicate that DE and Log K_{ow} are more suitable measures of polarity, as they better reflect molecular-level polarity, unlike WCA, which primarily measures superficial surface wettability. Regarding the classification of the ten studied MPs, most (PP, HDPE, LDPE, PS, EPS, PC, and PET) were easily distinguishable ($\Delta E > 10$), while limited distinguishability was observed between PA, ABS, and PVC ($\Delta E < 10$). The use of bandpass filters (green, yellow, orange and red) was demonstrated to isolate fluorescence behavior across selective wavelength bands, enabling differentiation based on their material-dependent spectral characteristics. It is suggested that combining different excitation wavelengths and selective transmission filters, powered by machine learning could overcome spectral overlaps and mitigate issues such as metamerism. With these advancements, this approach shows significant potential to establish NR fluorescence imaging as a standalone method for the accurate identification of MPs in large-scale environmental monitoring.

Abbreviations

HDPE: High-density polyethylene; LDPE: low-density polyethylene, PP: polypropylene; PS: polystyrene, EPS: Expanded polystyrene; ABS: acrylonitrile butadiene styrene; PC: polycarbonate; PVC: polyvinylchloride; PET: polyethylene terephthalate; PA: Polyamide; Hex: n-hexane; Chl: Chloroform; Ac: Acetone; Eth: Ethanol; Met: Methanol, Ac-Hex: Acetone with n-hexane; Ac-Eth: Acetone with ethanol, Ac-W: Acetone with water; NR: Nile Red; MPs: Microplastics; FI: Fluorescence intensity; NOM: Natural organic matter

Acknowledgements

We thank Dr. K.G. Karthikeyan for securing the funding (USDA NIFA Hatch Formula Funds (Project # WIS03059)) for this project and Dr. Majid Sarmadi for his expertise in color theory and polymer science.

Data Availability

The authors confirm that the data supporting the findings of this study are available within the article [and/or] its supplementary materials.

Disclosure of Interest

There are no conflicts of interest to declare

References

[1] H. Ritchie, V. Samborska, and M. Roser, "Plastic Pollution," *Our World in Data*, Nov. 2023, Accessed: Dec. 07, 2023. [Online]. Available: https://ourworldindata.org/plastic-pollution

[2] Y. Peng, P. Wu, A. T. Schartup, and Y. Zhang, "Plastic waste release caused by COVID-19 and its fate in the global ocean," *Proceedings of the National Academy of Sciences*, vol. 118, no. 47, p. e2111530118, Nov. 2021, doi: 10.1073/pnas.2111530118.

[3] U. N. Environment, "Plastic Pollution," UNEP - UN Environment Programme. Accessed: Dec. 07, 2023. [Online]. Available: http://www.unep.org/plastic-pollution

[4] L. Cai, J. Wang, J. Peng, Z. Wu, and X. Tan, "Observation of the degradation of three types of plastic pellets exposed to UV irradiation in three different environments," *Science of the Total Environment*, vol. 628, pp. 740–747, 2018.

[5] A. Paluselli, V. Fauvelle, F. Galgani, and R. Sempéré, "Phthalate Release from Plastic Fragments and Degradation in Seawater," *Environ. Sci. Technol.*, vol. 53, no. 1, pp. 166–175, Jan. 2019, doi: 10.1021/acs.est.8b05083.

[6] Y. K. Song, S. H. Hong, M. Jang, G. M. Han, S. W. Jung, and W. J. Shim, "Combined effects of UV exposure duration and mechanical abrasion on microplastic fragmentation by polymer type," *Environmental science & technology*, vol. 51, no. 8, pp. 4368–4376, 2017.

[7] H. Du, Y. Xie, and J. Wang, "Microplastic degradation methods and corresponding degradation mechanism: Research status and future perspectives," *Journal of Hazardous Materials*, vol. 418, p. 126377, Sep. 2021, doi: 10.1016/j.jhazmat.2021.126377.

[8] I. Peeken *et al.*, "Arctic sea ice is an important temporal sink and means of transport for microplastic," *Nat Commun*, vol. 9, no. 1, p. 1505, Apr. 2018, doi: 10.1038/s41467-018-03825-5.

[9] E. A. Hasenmueller, T. Baraza, N. F. Hernandez, and C. R. Finegan, "Cave sediment sequesters anthropogenic microparticles (including microplastics and modified cellulose) in subsurface environments," *Science of The Total Environment*, vol. 893, p. 164690, Oct. 2023, doi: 10.1016/j.scitotenv.2023.164690.

[10] I. E. Napper *et al.*, "Reaching New Heights in Plastic Pollution—Preliminary Findings of Microplastics on Mount Everest," *One Earth*, vol. 3, no. 5, pp. 621–630, Nov. 2020, doi: 10.1016/j.oneear.2020.10.020.

[11] A. J. Jamieson, L. S. R. Brooks, W. D. K. Reid, S. B. Piertney, B. E. Narayanaswamy, and T. D. Linley, "Microplastics and synthetic particles ingested by deep-sea amphipods in six of the deepest marine ecosystems on Earth," *Royal Society Open Science*, vol. 6, no. 2, p. 180667, Feb. 2019, doi: 10.1098/rsos.180667.

[12] B. Boots, C. W. Russell, and D. S. Green, "Effects of Microplastics in Soil Ecosystems: Above and Below Ground," *Environ. Sci. Technol.*, vol. 53, no. 19, pp. 11496–11506, Oct. 2019, doi: 10.1021/acs.est.9b03304.

[13] Y. Wan, C. Wu, Q. Xue, and X. Hui, "Effects of plastic contamination on water evaporation and desiccation cracking in soil," *Science of The Total Environment*, vol. 654, pp. 576–582, Mar. 2019, doi: 10.1016/j.scitotenv.2018.11.123.

[14] A. Menéndez-Pedriza and J. Jaumot, "Interaction of Environmental Pollutants with Microplastics: A Critical Review of Sorption Factors, Bioaccumulation and Ecotoxicological Effects," *Toxics*, vol. 8, no. 2, Art. no. 2, Jun. 2020, doi: 10.3390/toxics8020040.

[15] Y. Lee, J. Cho, J. Sohn, and C. Kim, "Health Effects of Microplastic Exposures: Current Issues and Perspectives in South Korea," *Yonsei Med J*, vol. 64, no. 5, pp. 301–308, May 2023, doi: 10.3349/ymj.2023.0048.
[16] G. O. Conti *et al.*, "Micro-and nano-plastics in edible fruit and vegetables. The first diet risks assessment for the general population," *Environmental Research*, vol. 187, p. 109677, 2020.
[17] A. Dehaut *et al.*, "Microplastics in seafood: Benchmark protocol for their extraction and characterization," *Environmental Pollution*, vol. 215, pp. 223–233, Aug. 2016, doi: 10.1016/j.envpol.2016.05.018.
[18] H. Lee, A. Kunz, W. J. Shim, and B. A. Walther, "Microplastic contamination of table salts from Taiwan, including a global review," *Sci Rep*, vol. 9, no. 1, p. 10145, Jul. 2019, doi: 10.1038/s41598-019-46417-z.
[19] A. Scircle and J. V. Cizdziel, "Detecting and Quantifying Microplastics in Bottled Water using Fluorescence Microscopy: A New Experiment for Instrumental Analysis and Environmental Chemistry Courses," *J. Chem. Educ.*, vol. 97, no. 1, pp. 234–238, Jan. 2020, doi: 10.1021/acs.jchemed.9b00593.
[20] M. Kedzierski, B. Lechat, O. Sire, G. Le Maguer, V. Le Tilly, and S. Bruzaud, "Microplastic contamination of packaged meat: Occurrence and associated risks," *Food Packaging and Shelf Life*, vol. 24, p. 100489, 2020.
[21] A. Ragusa *et al.*, "Plasticenta: First evidence of microplastics in human placenta," *Environ Int*, vol. 146, p. 106274, Jan. 2021, doi: 10.1016/j.envint.2020.106274.
[22] H. A. Leslie, M. J. M. van Velzen, S. H. Brandsma, A. D. Vethaak, J. J. Garcia-Vallejo, and M. H. Lamoree, "Discovery and quantification of plastic particle pollution in human blood," *Environment International*, p. 107199, Mar. 2022, doi: 10.1016/j.envint.2022.107199.
[23] L. Lebreton, M. Egger, and B. Slat, "A global mass budget for positively buoyant macroplastic debris in the ocean," *Sci Rep*, vol. 9, no. 1, Art. no. 1, Sep. 2019, doi: 10.1038/s41598-019-49413-5.
[24] A. Bakir *et al.*, "Creation of an international laboratory network towards global microplastics monitoring harmonisation," *Sci Rep*, vol. 14, no. 1, p. 12714, Jun. 2024, doi: 10.1038/s41598-024-62176-y.
[25] J.-L. Xu, K. V. Thomas, Z. Luo, and A. A. Gowen, "FTIR and Raman imaging for microplastics analysis: State of the art, challenges and prospects," *TrAC Trends in Analytical Chemistry*, vol. 119, p. 115629, Oct. 2019, doi: 10.1016/j.trac.2019.115629.
[26] C. Schwaferts, R. Niessner, M. Elsner, and N. P. Ivleva, "Methods for the analysis of submicrometer- and nanoplastic particles in the environment," *TrAC Trends in Analytical Chemistry*, vol. 112, pp. 52–65, Mar. 2019, doi: 10.1016/j.trac.2018.12.014.
[27] E. Fries, J. H. Dekiff, J. Willmeyer, M.-T. Nuelle, M. Ebert, and D. Remy, "Identification of polymer types and additives in marine microplastic particles using pyrolysis-GC/MS and scanning electron microscopy," *Environ. Sci.: Processes Impacts*, vol. 15, no. 10, p. 1949, 2013, doi: 10.1039/c3em00214d.
[28] W. Joon Shim, S. Hee Hong, and S. Eo Eo, "Identification methods in microplastic analysis: a review," *Analytical Methods*, vol. 9, no. 9, pp. 1384–1391, 2017, doi: 10.1039/C6AY02558G.

[29] D. Ho, S. Liu, and H. Wei, “The glowing potential of Nile red for microplastics Identification: Science and mechanism of fluorescence staining,” *Microchemical Journal*, p. 109708, 2023.
[30] D. Kalaronis *et al.*, “Microscopic techniques as means for the determination of microplastics and nanoplastics in the aquatic environment: A concise review,” *Green Analytical Chemistry*, vol. 3, p. 100036, Dec. 2022, doi: 10.1016/j.greeac.2022.100036.
[31] B. Singh and A. Kumar, “Advances in microplastics detection: A comprehensive review of methodologies and their effectiveness,” *TrAC Trends in Analytical Chemistry*, vol. 170, p. 117440, Jan. 2024, doi: 10.1016/j.trac.2023.117440.
[32] A. B. Silva, A. S. Bastos, C. I. Justino, J. P. da Costa, A. C. Duarte, and T. A. Rocha-Santos, “Microplastics in the environment: Challenges in analytical chemistry-A review,” *Analytica chimica acta*, vol. 1017, pp. 1–19, 2018.
[33] J. Rumin *et al.*, “The use of fluorescent Nile red and BODIPY for lipid measurement in microalgae,” *Biotechnol Biofuels*, vol. 8, no. 1, p. 42, 2015, doi: 10.1186/s13068-015-0220-4.
[34] C. Wang, L. Jiang, R. Liu, M. He, X. Cui, and C. Wang, “Comprehensive assessment of factors influencing Nile red staining: Eliciting solutions for efficient microplastics analysis,” *Marine Pollution Bulletin*, vol. 171, p. 112698, Oct. 2021, doi: 10.1016/j.marpolbul.2021.112698.
[35] T. Maes, R. Jessop, N. Wellner, K. Haupt, and A. G. Mayes, “A rapid-screening approach to detect and quantify microplastics based on fluorescent tagging with Nile Red,” *Sci Rep*, vol. 7, no. 1, p. 44501, Mar. 2017, doi: 10.1038/srep44501.
[36] M. T. Sturm, H. Horn, and K. Schuhen, “The potential of fluorescent dyes—comparative study of Nile red and three derivatives for the detection of microplastics,” *Anal Bioanal Chem*, vol. 413, no. 4, pp. 1059–1071, Feb. 2021, doi: 10.1007/s00216-020-03066-w.
[37] W. J. Shim, Y. K. Song, S. H. Hong, and M. Jang, “Identification and quantification of microplastics using Nile Red staining,” *Marine Pollution Bulletin*, vol. 113, no. 1, pp. 469–476, Dec. 2016, doi: 10.1016/j.marpolbul.2016.10.049.
[38] M. Tamminga, E. Hengstmann, and E. Fischer, “Nile Red Staining as a Subsidiary Method for Microplastic Quantification: A Comparison of Three Solvents and Factors Influencing Application Reliability,” *Journal of Earth Sciences & Environmental Studies*, Feb. 2017.
[39] G. Erni-Cassola, M. I. Gibson, R. C. Thompson, and J. A. Christie-Oleza, “Lost, but Found with Nile Red: A Novel Method for Detecting and Quantifying Small Microplastics (1 mm to 20 μm) in Environmental Samples,” *Environ. Sci. Technol.*, vol. 51, no. 23, pp. 13641–13648, Dec. 2017, doi: 10.1021/acs.est.7b04512.
[40] H. A. Nel *et al.*, “Detection limits are central to improve reporting standards when using Nile red for microplastic quantification,” *Chemosphere*, vol. 263, p. 127953, Jan. 2021, doi: 10.1016/j.chemosphere.2020.127953.
[41] C. Campanale, I. Savino, I. Pojar, C. Massarelli, and V. F. Uricchio, “A Practical Overview of Methodologies for Sampling and Analysis of Microplastics in Riverine Environments,” *Sustainability*, vol. 12, no. 17, Art. no. 17, Jan. 2020, doi: 10.3390/su12176755.
[42] J. Masura, J. Baker, G. Foster, and C. Arthur, “Laboratory Methods for the Analysis of Microplastics in the Marine Environment: Recommendations for quantifying synthetic particles in waters and sediments.,” NOAA Marine Debris Division, Report, 2015. doi: 10.25607/OBP-604.

[43] S. I. S. Inc a division of Diagnostic Instruments, “Color Space - SPOT Imaging,” SPOT Imaging Solutions. Accessed: Dec. 01, 2022. [Online]. Available: http://wwww.spotimaging.com
[44] K. Sebők-Nagy and L. Biczók, “Effect of hydrogen-bonding on the fluorescent properties of Nile Red and N-(4-pyridyl)-1,2-naphthalimide,” *Magyar Kemiai Folyoirat, Kemiai Kozlemenyek*, vol. 109–110, pp. 29–33, Mar. 2004.
[45] A. Ikeda, C. Abe, W. Matsuura, and Y. Hasegawa, “Development of Methanol Permselective FAU-Type Zeolite Membranes and Their Permeation and Separation Performances,” *Membranes*, vol. 11, no. 8, Art. no. 8, Aug. 2021, doi: 10.3390/membranes11080627.
[46] E. Ghobadi *et al.*, “The Influence of Water and Solvent Uptake on Functional Properties of Shape-Memory Polymers,” *International Journal of Polymer Science*, vol. 2018, p. e7819353, May 2018, doi: 10.1155/2018/7819353.
[47] S. Konde, J. Ornik, J. A. Prume, J. Taiber, and M. Koch, “Exploring the potential of photoluminescence spectroscopy in combination with Nile Red staining for microplastic detection,” *Marine Pollution Bulletin*, vol. 159, p. 111475, Oct. 2020, doi: 10.1016/j.marpolbul.2020.111475.
[48] J. Burke, “Solubility Parameters: Theory and Application.” Accessed: Oct. 08, 2022. [Online]. Available: https://cool.culturalheritage.org/coolaic/sg/bpg/annual/v03/bp03-04.html
[49] “Surface Free Energy Components by Polar/Dispersion and Acid—Base Analyses; and Hansen Solubility Parameters for Various Polymers.” Accessed: Dec. 01, 2023. [Online]. Available: https://www.accudynetest.com/polytable_02.html
[50] “Critical Surface Tension and Contact Angle with Water for Various Polymers (sort by contact angle).” Accessed: Dec. 01, 2023. [Online]. Available: https://www.accudynetest.com/polytable_03.html?sortby=contact_angle
[51] T. Zedníček, “What is a Dielectric Constant of Plastic Materials ?,” Passive Components Blog. Accessed: Dec. 01, 2023. [Online]. Available: https://passive-components.eu/what-is-dielectric-constant-of-plastic-materials/
[52] K. Min, J. D. Cuiffi, and R. T. Mathers, “Ranking environmental degradation trends of plastic marine debris based on physical properties and molecular structure,” *Nat Commun*, vol. 11, no. 1, Art. no. 1, Feb. 2020, doi: 10.1038/s41467-020-14538-z.
[53] S. P. Farnand, “Using [Delta] E metrics for measuring color difference in hard copy pictorial images,” in *Color Imaging VIII: Processing, Hardcopy, and Applications*, SPIE, 2003, pp. 109–118.
[54] “Delta E ≦2 Color Accuracy.” Accessed: Dec. 05, 2023. [Online]. Available: https://www.viewsonic.com/colorpro/articles/detail/deltae2color-accuracy_3
[55] S. Hoekstra, “How do you Measure Color Accuracy?,” Nix Sensor Ltd. Accessed: Dec. 05, 2023. [Online]. Available: https://www.nixsensor.com/blog/measure-color-accuracy/
[56] J. Best, *Colour Design: Theories and Applications*. Woodhead Publishing, 2017.
[57] J. Lin, D. Yan, J. Fu, Y. Chen, and H. Ou, “Ultraviolet-C and vacuum ultraviolet inducing surface degradation of microplastics,” *Water Research*, vol. 186, p. 116360, Nov. 2020, doi: 10.1016/j.watres.2020.116360.
[58] B. I. Chaudhary, C. L. Liotta, J. M. Cogen, and M. Gilbert, “Plasticized PVC,” in *Reference Module in Materials Science and Materials Engineering*, Elsevier, 2016. doi: 10.1016/B978-0-12-803581-8.02631-X.

[59] Z. Ahmad and Z. Ahmad, *Polymer Dielectric Materials*. IntechOpen, 2012. doi: 10.5772/50638.
[60] "Delocalization of Electrons," Chemistry LibreTexts. Accessed: Feb. 14, 2024. [Online]. Available: https://chem.libretexts.org/Bookshelves/Physical_and_Theoretical_Chemistry_Textbook_Maps/Supplemental_Modules_(Physical_and_Theoretical_Chemistry)/Chemical_Bonding/Valence_Bond_Theory/Delocalization_of_Electrons
[61] T. Yasuda, T. Okuno, and H. Yasuda, "Contact Angle of Water on Polymer Surfaces," *Langmuir*, vol. 10, no. 7, pp. 2435–2439, Jul. 1994, doi: 10.1021/la00019a068.
[62] M. Van Melkebeke, C. Janssen, and S. De Meester, "Characteristics and Sinking Behavior of Typical Microplastics Including the Potential Effect of Biofouling: Implications for Remediation," *Environ. Sci. Technol.*, vol. 54, no. 14, pp. 8668–8680, Jul. 2020, doi: 10.1021/acs.est.9b07378.
[63] C. Rayssi, S. El.Kossi, J. Dhahri, and K. Khirouni, "Frequency and temperature-dependence of dielectric permittivity and electric modulus studies of the solid solution Ca 0.85 Er 0.1 Ti 1−x Co 4x/3 O 3 ($0 \leq x \leq 0.1$)," *RSC Advances*, vol. 8, no. 31, pp. 17139–17150, 2018, doi: 10.1039/C8RA00794B.
[64] F. P. La Mantia and R. Schifani, "Natural weathering of low density polyethylene: Part 2—Dielectric properties," *Polymer Degradation and Stability*, vol. 10, no. 1, pp. 67–78, Jan. 1985, doi: 10.1016/0141-3910(85)90021-7.
[65] "Dielectric Properties." Accessed: Oct. 08, 2022. [Online]. Available: https://polymerdatabase.com/polymer%20physics/Permitivity.html
[66] "Dielectric Constant: Definition, Units, Formula, Plastic Values &Material List." Accessed: Nov. 25, 2022. [Online]. Available: https://omnexus.specialchem.com/polymer-properties/properties/dielectric-constant
[67] J. R. Lakowicz, *Topics in Fluorescence Spectroscopy: Principles*. Springer Science & Business Media, 2006.
[68] K. N. Fotopoulou and H. K. Karapanagioti, "Degradation of Various Plastics in the Environment," in *Hazardous Chemicals Associated with Plastics in the Marine Environment*, H. Takada and H. K. Karapanagioti, Eds., in The Handbook of Environmental Chemistry. , Cham: Springer International Publishing, 2019, pp. 71–92. doi: 10.1007/698_2017_11.
[69] N. Meyers *et al.*, "Microplastic detection and identification by Nile red staining: Towards a semi-automated, cost- and time-effective technique," *Science of The Total Environment*, vol. 823, p. 153441, Jun. 2022, doi: 10.1016/j.scitotenv.2022.153441.
[70] S. Prasad, A. Bennett, and M. Triantafyllou, *Characterization of Nile Red-Stained Microplastics through Fluorescence Spectroscopy*. 2024. doi: 10.20944/preprints202407.2045.v1.